Science Advances
AAAS

advances.sciencemag.org/cgi/content/full/6/30/eaba5379/DC1

Supplementary Materials for

Switching the intracellular pathway and enhancing the therapeutic efficacy of small interfering RNA by auroliposome

Md. Nazir Hossen, Lin Wang, Harisha R. Chinthalapally, Joe D. Robertson, Kar-Ming Fung, Stefan Wilhelm, Magdalena Bieniasz, Resham Bhattacharya, Priyabrata Mukherjee*

*Corresponding author. Email: priyabrata-mukherjee@ouhsc.edu

Published 22 July 2020, *Sci. Adv.* **6**, eaba5379 (2020)
DOI: 10.1126/sciadv.aba5379

This PDF file includes:

Figs. S1 to S9

A

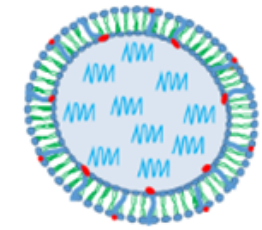

siRNA

Phospholipid bilayer (DOTAP and DOPE, 1:1)

Tween 20

siRNA-liposomes (siRNA-cLPs)

B

DOTAP (Cationic Charge)

1,2-dioleoyl-3-trimethylammonium-propane (chloride salt)

DOPE (Neutral lipid)

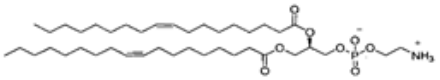

1,2-dioleoyl-*sn*-glycero-3-phosphoethanolamine

DOPC (Anionic lipid)

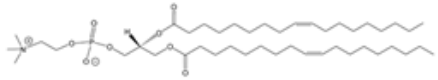

1,2-dioleoyl-*sn*-glycero-3-phosphocholine

PE-PEG (Anionic charge)

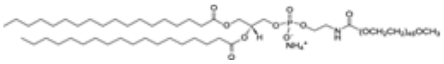

1,2-distearoyl-*sn*-glycero-3-phosphoethanolamine-N [methoxy (polyethylene glycol)-2000] (ammonium salt)

C

Formulation ID	Lipid Compositions	Ratio of Lipid (w/w)	Lipid/siRNA (w/w) ratio
E-LPs	DOTAP:DOPE	50:50	25:0
F1	DOTAP:DOPC	50:50	25:1
F2	DOTAP:DOPE :DOPC	40:10:50	25:1
F3	DOTAP:DOPE :DOPC	30:30:40	25:1
F4	DOTAP:DOPE :DOPC:PE-PEG	30:10:40: 20	25:1
F5	DOTAP:DOPE :DOPC:PE-PEG	30:20:40: 10	25:1
F6	DOTAP:DOPE :DOPC:PE-PEG	30:25:40: 5	25:1
F7	DOTAP:DOPE	50:50	25:1
F8	DOTAP:DOPE :PE-PEG	50:50:0.1 25mol%	25:1
F9	DOTAP:DOPE :PE-PEG	50:50:0.2 5mol%	25:1
F10	DOTAP:DOPE :PE-PEG	50:50:0.5 mol%	25:1

D

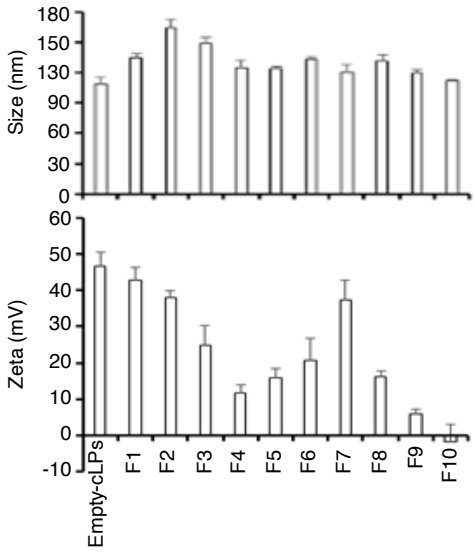

E

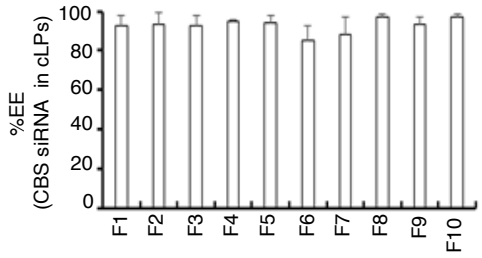

F

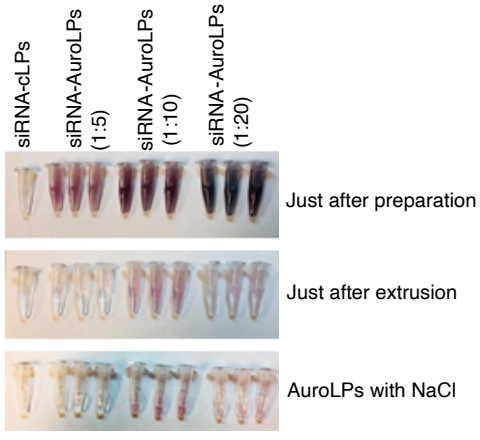

fig. S1. Compositions and physicochemical characterization of liposomal formulations. (**A**) Schematic representation of siRNA-cLPs. (**B**) Chemical structure of utilized lipids for the formulation of siRNA-LPs. (**C**) Modulation of lipid compositions for the preparation of siRNA-LPs. (**D**) The size and zeta potential of CBS-siRNA-LPs, as denoted by F1, F2, F3, F4, F5, F6, F7, F8, F9, F10 and empty-LPs were measured by dynamic light scatter microscopy (DLS). (**E**) Entrapment of CBS-siRNA into LPs was measured using Ribogreen assay (n=3). (**F**) The photographs showed the optimization of ratio of siRNA/AuNP. Photo credit: M. N. Hossen (Oklahoma University Health Science Centre).

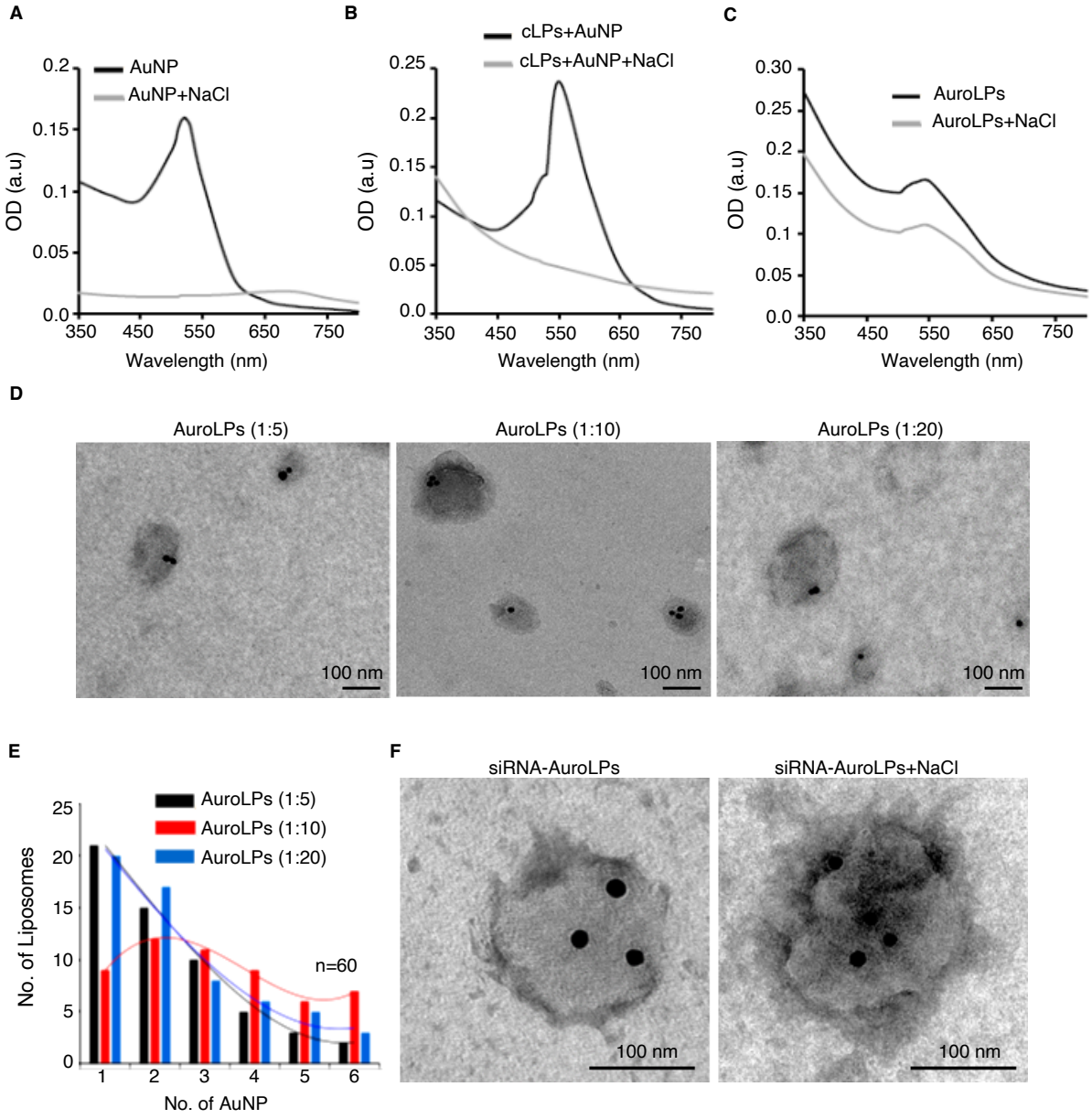

fig. S2. Aggregation study of AuroLPs using UV-vis and transmission electron microscopy (TEM). (A-C) UV-Vis spectrum of without or with NaCl of AuNP, cLPs+AuNP and AuroLPs. (D) 0.2% uranyl acetate (UA) stained auroliposomes at various ratio of siRNA/AuNP (1:5; 1:10 and 1:20) that were visualized under TEM and its corresponding number of AuNP in auroliposomal formulations (n=60 of each ratio) (E). (F) TEM images of AuroLPs and AuroLPs+NaCl. Scale bar: 100 nm.

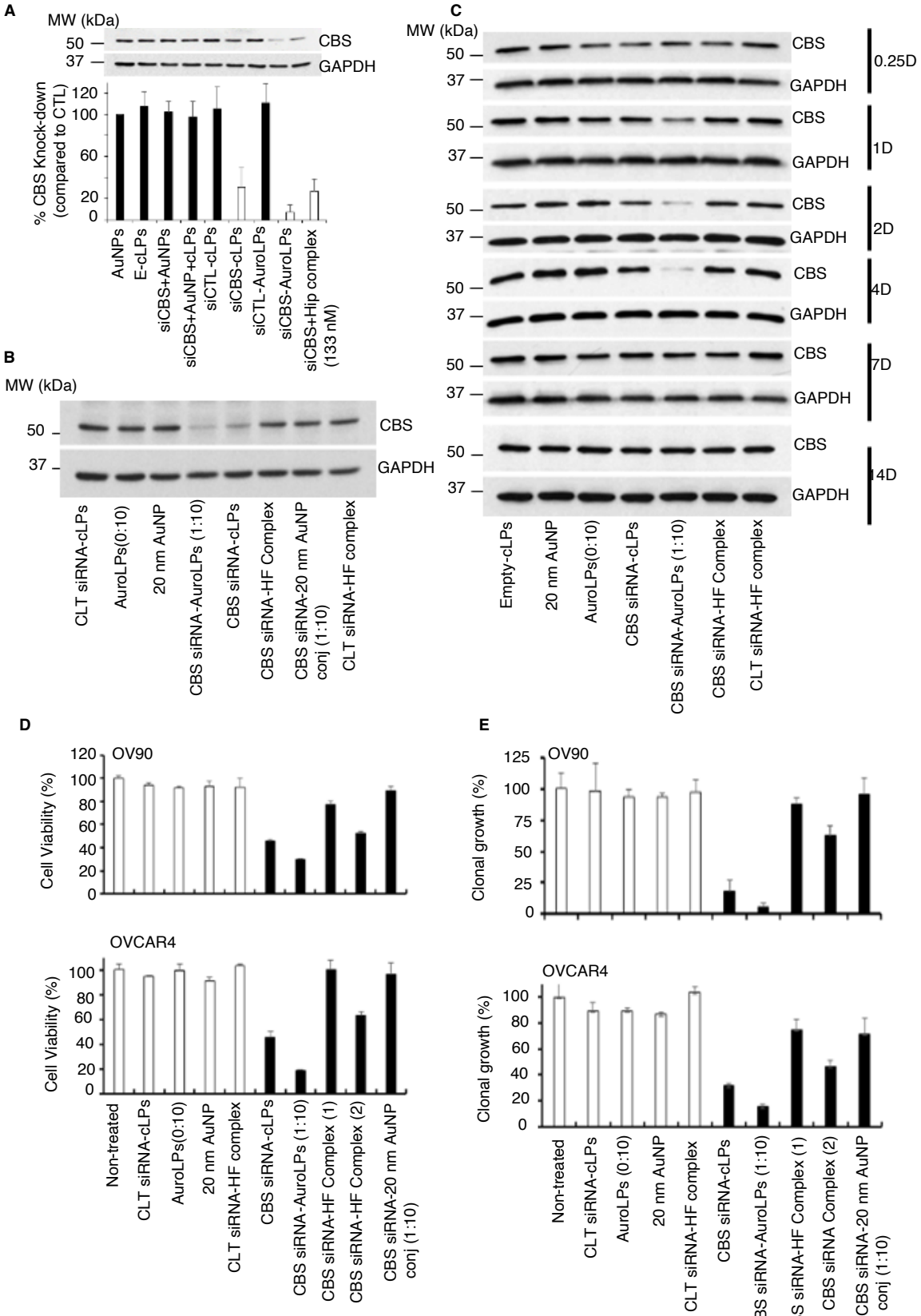
A
MW (kDa)
50
37
CBS
GAPDH
% CBS Knock-down (compared to CTL)
120
100
60
20
0
AuNPs
E-cLPs
siCBS+AuNPs
siCBS+AuNP+cLPs
siCTL-cLPs
siCBS-cLPs
siCTL-AuroLPs
siCBS-AuroLPs
siCBS+Hip complex (133 nM)
B
MW (kDa)
50
37
CBS
GAPDH
CLT siRNA-cLPs
AuroLPs(0:10)
20 nm AuNP
CBS siRNA-AuroLPs (1:10)
CBS siRNA-cLPs
CBS siRNA-HF Complex
CBS siRNA-20 nm AuNP conj (1:10)
CLT siRNA-HF complex
C
MW (kDa)
50
37
CBS
GAPDH
0.25D
1D
2D
4D
7D
14D
Empty-cLPs
20 nm AuNP
AuroLPs(0:10)
CBS siRNA-cLPs
CBS siRNA-AuroLPs (1:10)
CBS siRNA-HF Complex
CLT siRNA-HF complex
D
OV90
Cell Viability (%)
120
100
80
60
40
20
0
OVCAR4
Cell Viability (%)
100
80
60
40
20
0
Non-treated
CLT siRNA-cLPs
AuroLPs(0:10)
20 nm AuNP
CLT siRNA-HF complex
CBS siRNA-cLPs
CBS siRNA-AuroLPs (1:10)
CBS siRNA-HF Complex (1)
CBS siRNA-HF Complex (2)
CBS siRNA-20 nm AuNP conj (1:10)
E
OV90
Clonal growth (%)
125
100
75
50
25
0
OVCAR4
Clonal growth (%)
100
80
60
40
20
0
Non-treated
CLT siRNA-cLPs
AuroLPs (0:10)
20 nm AuNP
CLT siRNA-HF complex
CBS siRNA-cLPs
CBS siRNA-AuroLPs (1:10)
CBS siRNA-HF Complex (1)
CBS siRNA Complex (2)
CBS siRNA-20 nm AuNP conj (1:10)

fig. S3. Silencing and its stability and viability of cancer cells as a function of CBS-siRNA-AuroLPs treatment. (**A**) Silencing activity of CBS-siRNA-AuroLPs. OV90 (2 x 10^5) were cultured overnight in the presence of 10% FBS media and were then treated with AuNPs, empty-cLPs, AuNP+CBS-siRNA, AuNP+CBS-siRNA+empty-cLPs, control siRNA-cLPs, control siRNA-AuroLPs, CBS-siRNA-AuroLPs, and CBS-siRNA-cLPs at a final siRNA dose of 25 nM, whereas complex (133 nM) at a final concentration of 133 nM siRNA. A 48h post incubation, the extent of CBS silencing was determined at the protein level by western blot. GAPDH was used as a loading control. (**B**) Silencing activity of CBS-siRNA-AuroLPs. OVCAR4 cells (2 x 10^5) were cultured overnight in the presence of 10% FBS media and were then treated with control siRNA-cLPs, AuroLPs, 20 nm AuNP, CBS-siRNA-AuroLPs, CBS-siRNA-cLPs, complex and conjugate at a final concentration of 25nM siRNA. A 48h post incubation, the extent of CBS silencing was determined at the protein level by western blot. GAPDH was used as a loading control. (**C**) Stability of silencing activity. OVCAR4 cells (2 x 10^5) were cultured overnight in the presence of 10% FBS media and were then treated with AuroLPs, 20 nm AuNP, CBS-siRNA-AuroLPs, CBS-siRNA-cLPs, complex, control siRNA complex and empty-cLPs at a final concentration of 25 nM siRNA. A 6h, 1D, 2D, 4D, 7D and 14D post incubation, the extent of CBS silencing was determined at the protein level by western blot. GAPDH was used as a loading control. (**D**) Cell viability. Cells (OVCAR4 and OV90) were grown in 96 well plate at a density of 3000 cells/ well overnight and were then treated either control siRNA-cLPs, AuroLPs, 20 nm AuNP, CBS-siRNA-AuroLPs, CBS-siRNA-cLPs, complex and conjugate at the same dose or complex at a dose of 133 nM or remains untreated. Post 48h cells viability was measured by MTT assay (n=6). (**E**) Clonal growth. OVCAR4 and OV90 cells (200 cells/well in 6 cm dish) were co-transfected with either control siRNA-cLPs, AuroLPs, 20 nm AuNP, CBS-siRNA-AuroLPs, CBS-siRNA-cLPs, complex

and conjugate at the same dose or complex at a dose of 133 nM or remains untreated. After 12 (OVCAR4) or 8 (OV90) days, colonies were stained with crystal violet, imaged and counted by using colony counter machine (n=3).

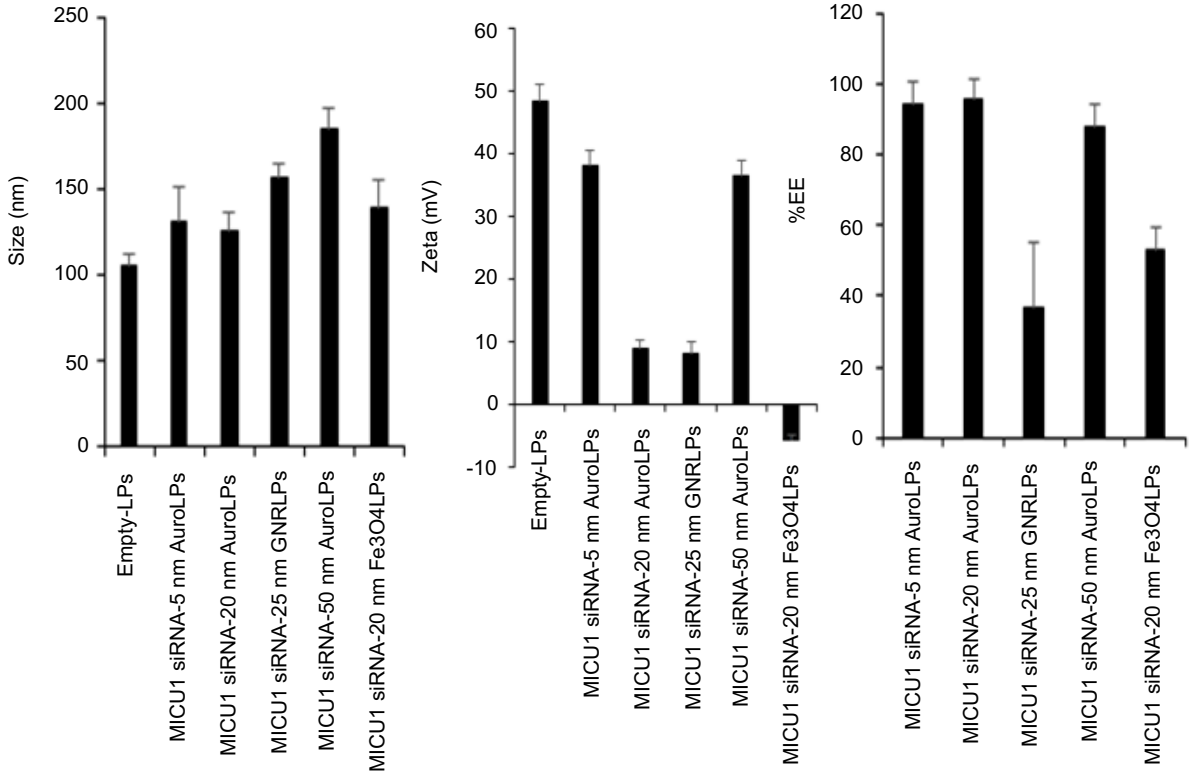

fig. S4. Physicochemical characterizations and encapsulation efficiency of siRNA-AuroLPs and Fe3O4LPs. (**A-B**) The size and zeta potential of empty-cLPs, siRNA-5 nm AuroLPs (oval), siRNA-AuroLPs (oval), siRNA-50 nm AuroLPs (oval), siRNA-25 nm AuroLPs (rod) and siRNA-20 nm Fe3O4LPs (oval) were measured by dynamic light scatter microscopy (DLS). (**C**) Entrapment efficiency of MICU1-siRNA into 5 nm AuroLPs (oval), AuroLPs (oval), 50 nm AuroLPs (oval), 25 nm AuroLPs (rod) and 20 nm Fe3O4LPs (oval) was determined by using ribogreen assay (n=3).

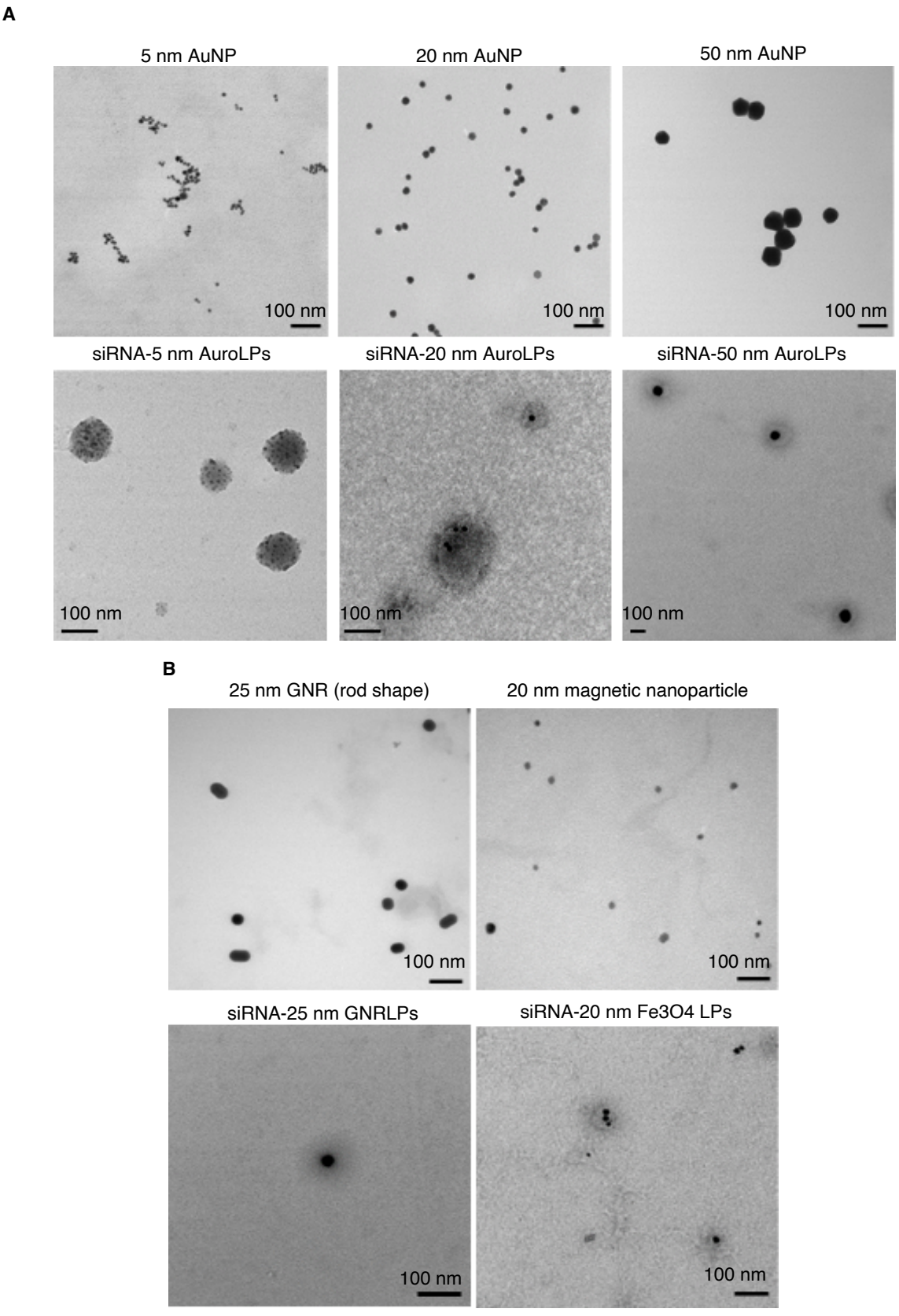
A
5 nm AuNP
20 nm AuNP
50 nm AuNP
100 nm
100 nm
100 nm
siRNA-5 nm AuroLPs
siRNA-20 nm AuroLPs
siRNA-50 nm AuroLPs
100 nm
100 nm
100 nm
B
25 nm GNR (rod shape)
20 nm magnetic nanoparticle
100 nm
100 nm
siRNA-25 nm GNRLPs
siRNA-20 nm Fe3O4 LPs
100 nm
100 nm

fig. S5. Morphological observation of different Auros, AuroLPs, Fe3O4 and FeO4LPs. The morphology of 5 nm AuNP, siRNA-5 nm AuroLPs (oval), 20 nm AuNP, siRNA-AuroLPs (oval), 50 nm AuNP, siRNA-50 nm AuroLPs (oval), 25 nm GNR (rod shape), siRNA-25 nm AuroLPs (rod), 20 nm Fe3O4 (oval) and siRNA-20 nm Fe3O4LPs was visualized by using TEM. Scale bar 100 μm.

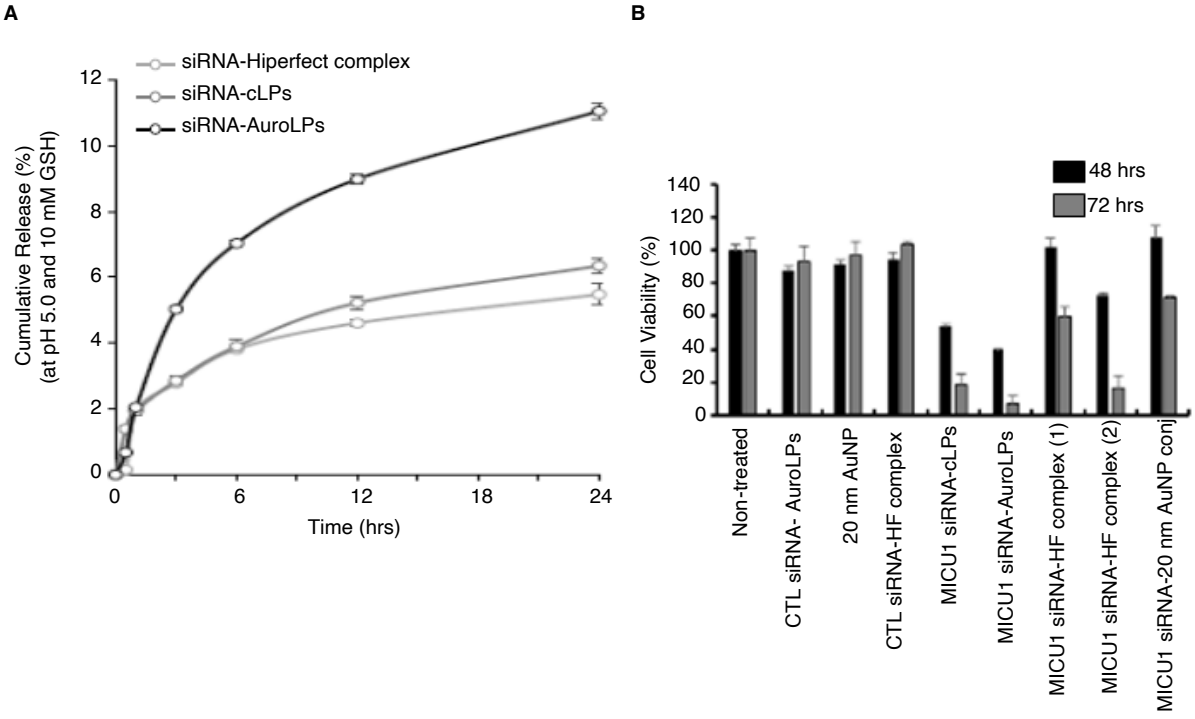

fig. S6. siRNA release and cell viability of MICU1-siRNA-loaded AuroLPs. (**A**) The release of siRNA from cLPs AuroLPs and siRNA-HF complex at a lysosomal environment (acidic pH and high GSH) was measured at 15 and 30 mins, 1, 3, 6, 12 and 24h using ribogreen assay. (**B**) Cell viability. Cells were treated with control siRNA-AuroLPs, 20 nm AuNP, CTL-siRNA complex, MICU1-siRNA-AuroLPs, MICU1-siRNA-cLPs, complex (1) (50 nM) or complex (2) (133 nM) and conjugate at a final concentration of 50 nM siRNA. Post 48 and 72 hrs, cell viability was measured by MTT assay (n=5)

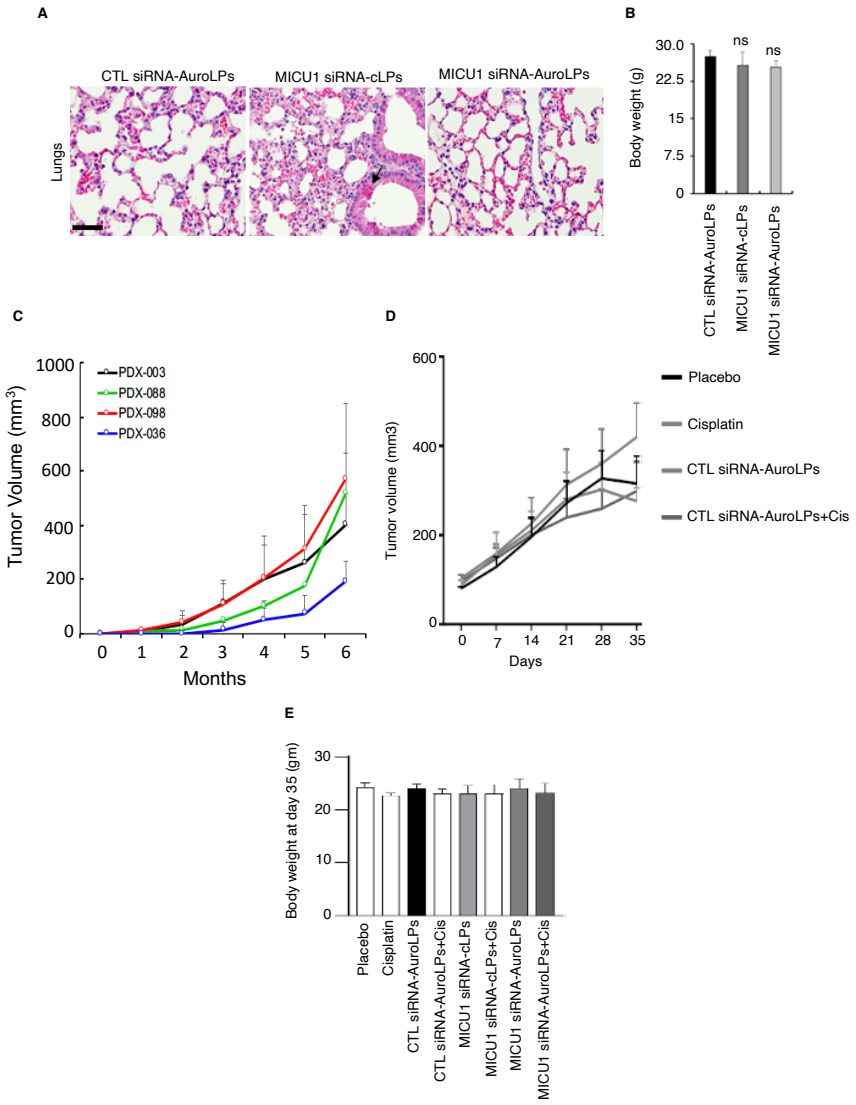

fig. S7. Tumor growth rate of PDX model mice and therapeutic and toxicological analysis of AuroLPs in vivo. (**A**) Tissues from lungs of mice treated with CTL-siRNA-AuroLPs, MICU1-siRNA-cLPs and MICU1-siRNA-AuroLPs were collected, fixed with formalin and sectioned at 5 µm in size. The representative H&E stained sections of lungs from CTL-siRNA-AuroLPs, MICU1-siRNA-cLPs and MICU1siRNA-AuroLPs groups were shown, where black arrow head indicates inflammatory cells accumulation in lung of siMICU1-cLPs group. Images were captured by Nikon Eclipse Ni Microscope. Scale bar is 50 µm. (C) Tumor growth rate of ovarian cancer PDXs. Graph represents epithelial ovarian PDX growth rate in NOD/SCID mice. Animals were

subcutaneously implanted with PDX fragment and tumor growth rate was monitored for 6 months. (**B**) Body weight of mice after treatment (OV90 cell line-derived xenograft). (**D**) The control groups including placebo (PBS), cisplatin (0.5 mg/kg), CTL-siRNA-AuroLPs or in combination with i.p injection of cisplatin (0.5 mg/kg). (E) The body weight of PDX mice at 35-day was shown.

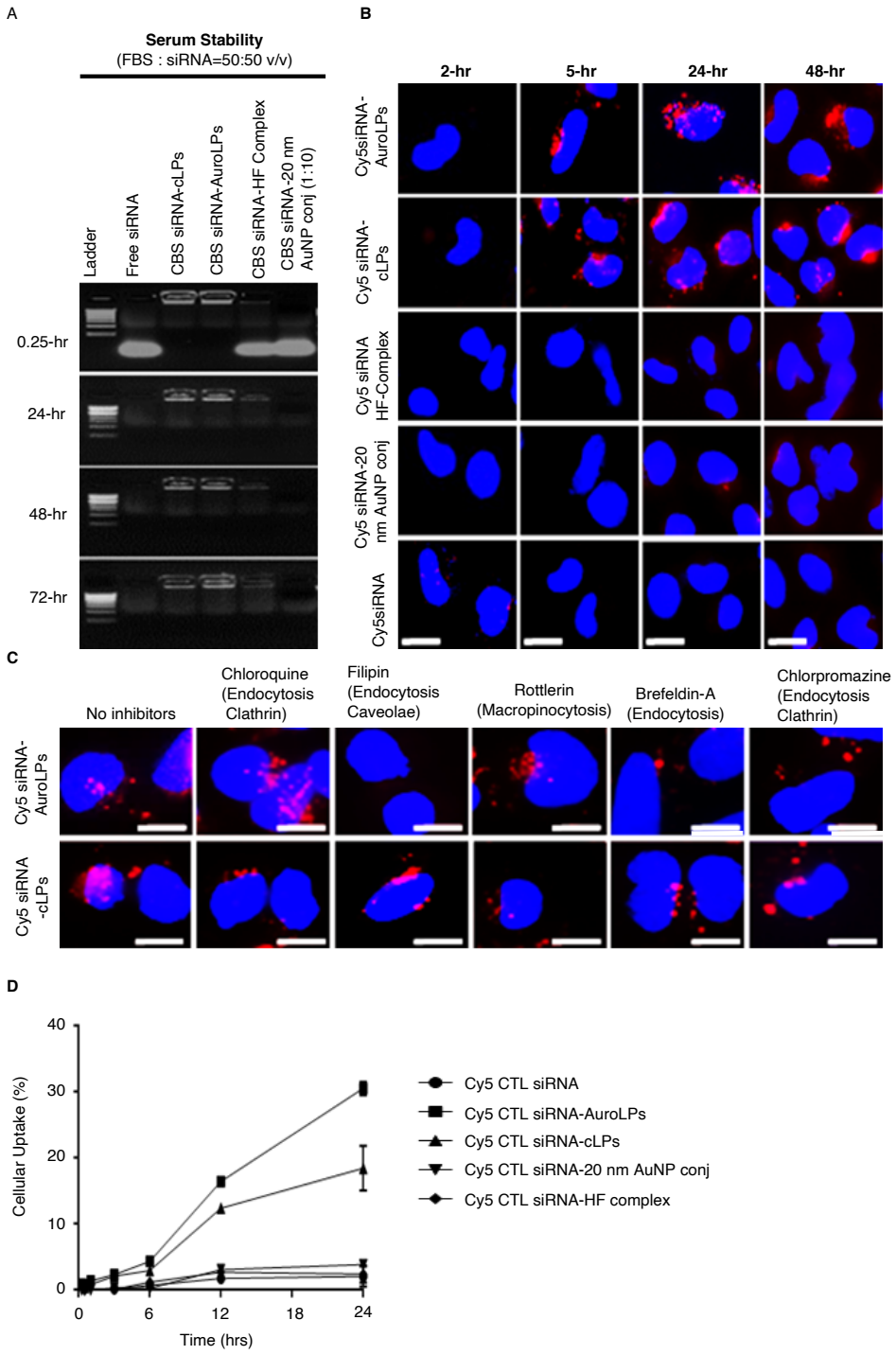

fig. S8. Stability, cellular uptake and mechanism of uptake for AuroLPs. (**A**) Serum stability of CBS-siRNA-AuroLPs. CBS-siRNA, CBS-siRNA-cLPs, CBS-siRNA-AuroLPs, complex (Hiperfect+CBS-siRNA) and conjugate (20 nm AuNP + CBS-siRNA) (1 µg each) were incubated with 100% FBS (1:1 v/v) at 37ºC for 15 mins, 24, 48 and 72 h and 1.5% agarose gel electrophoresis was performed in the presence of TBE buffer. (**B**) Time-dependent cellular uptake of fluorescence labeled siRNA-AuroLPs. Cells were treated with Cy5 siRNA, Cy5 siRNA-LPs, Cy5 siRNA-AuroLPs, conjugate and complex at a dose of 25 nM siRNA. At various time points (2, 5, 24 and 48 h), these cells were fixed, stained nuclei with DAPI and were then visualized by fluorescence microscopy. (**C**) Quantitative cellular uptake of AuroLPs. At the same conditions, cells were incubated with Cy5 siRNA, Cy5 siRNA-cLPs, Cy5 siRNA-AuroLPs, complex and conjugate at a final concentration of 25 nM siRNA. The fluorescence intensity of Cy5 siRNA in cell lysate was quantified by using a CLARIOstar plate reader. (**D**) Uptake mechanism of AuroLPs. Cells were treated with either the presence or the absence of chemical inhibitors, including chlorpromazine, chloroquine, filipin, rottlerin and brefeldin. Post 2-hr, Cy5 CTL-siRNA-cLPs and Cy5 CTL-siRNA-AuroLPs (25 nM CTL-siRNA) were further incubated for 4 hr. These fixed cells were mounted with media containing DAPI and were then visualized under fluorescence microscope. Scale bar 10 um.

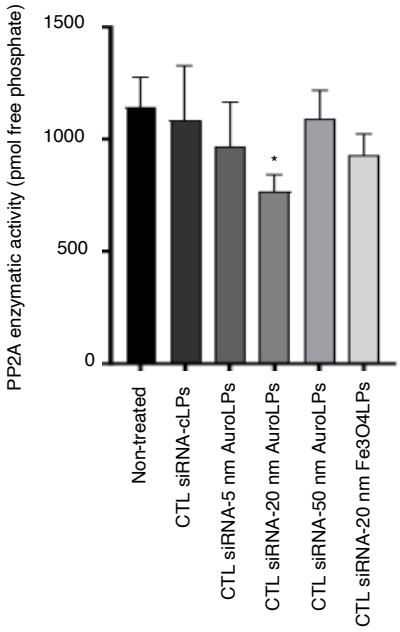

fig. S9. Measurement of protein phosphatase 2A (PP2A) enzymes in cell cytosol using immunoprecipitation assay. Cells were incubated with either CTL-siRNA-cLPs, CTL-siRNA-5 nm AuroLPs, -20 nm AuroLPs, -50 nm AuroLPs, -Fe3O4cLPs or remained non-treated for 15 mins. From cell lysates, PP2A proteins were immunoprecipitated and the absorbance, as a read out of PP2A enzymatic activity, was measured at 650 nm by using a CLARIOstar plate reader. The statistical analysis was performed by One-way ANOVA followed by dunnetts' multiple comparison test, mean±s.d, *$p<0.05$, n=4.